IEEE Access
Multidisciplinary | Rapid Review | Open Access Journal

Received 17 November 2023, accepted 7 December 2023, date of publication 12 December 2023,
date of current version 15 December 2023.

Digital Object Identifier 10.1109/ACCESS.2023.3341505

METHODS

A Short Time Expansion Measurement Method for the Detection of Aging Effect of Lithium Ion Cells Using a High Resolution Laser Interfometric Setup

SEBASTIAN GIELINGER, THIEMO HEIN, ANDREAS ZIEGLER, DAVID OESER, SEBASTIAN BREITFELDER, AND GUNTHER BOHN

Technology Transfer Center for Electromobility (TTZ-EMO), Technical University of Applied Sciences Würzburg-Schweinfurt, 97616 Bad Neustadt an der Saale, Germany

Corresponding author: Sebastian Gielinger (sebastian.gielinger@thws.de)

ABSTRACT In this work a new expansion measurement methodology for the detection of ageing mechanisms in lithium ion cells is described and evaluated. For this purpose, a polarization-optical homodyne Michelson interferometer with a resolution of approx. 10 nm was set up to allow measurements of different cell types, cell sizes, and cell chemistry within a Memmert IP55 climate chamber. The used interferometric measurement setup is ten times more accurate than measurement systems commonly used for battery measurements in the literature. The better spatial resolution of an interferometer setup enables the recording of the expansion response to short current pulses with low transferred charge. This offers the possibility to detect ageing mechanisms such as lithium plating within short measuring times. With this measurement setup, a lithium iron phosphate pouch cell from the company A123, with the model identification AMP20M1HD-A, is measured. First, an expansion measurement over a full charge and discharge cycle with a constant load of $\pm\frac{C}{20}(\widehat{=}1\,\mathrm{A})$ is performed. Here, the cell undergoes an expansion of about 42 µm. Subsequently, the in this work proposed measurement methodology is presented to show the influence of effects such as the formation of overshooting graphite stages or lithium plating on cell expansion. For this purpose, at a residual capacitance of 50%, the cell is pulsed with current of different intensity $I \in \{\pm 20\,\mathrm{A}, \pm 80\,\mathrm{A}\}$ for $t = \{240\,\mathrm{s}, 60\,\mathrm{s}\}$, at $T = \{10\,^{\circ}\mathrm{C}, 20\,^{\circ}\mathrm{C}, 30\,^{\circ}\mathrm{C}\}$, respectively, and the mechanical response is recorded using the high accuracy interferometer setup. A mechanical relaxation of the cell after the pulses with a time constant in the range between 10 s and 20 s can be observed. It is shown that this relaxation behavior can be associated with effects of the anode known from the literature, such as the formation of overshooting graphite stages or lithium plating. These effects can be recorded by the very high-resolution measurement already with little transferred charge and within a short measurement time.

INDEX TERMS Lithium-ion cell, expansion measurement, interferometer, lithium plating, lithium iron phosphate, graphite anode.

I. INTRODUCTION

Due to the constantly evolving electrification of vehicles and devices of all kinds, the demand for efficient, powerful, and safe energy storage systems has grown continuously in the last few years [1]. For this purpose, lithium-ion batteries have been used commercially since 1991 for their high energy density, voltage stability, and long lifetime. The group of lithium-ion batteries is formed by a whole series of different cell chemistries. These cell chemistries differ mainly in their cathode material and meet different requirements specific to their application [2]

The associate editor coordinating the review of this manuscript and approving it for publication was Wuliang Yin.

It is known that lithium-ion cells undergo a reversible volume change during a charge and discharge cycle. This reversible volume change is caused by a redistribution of lithium ions within the active materials during the charge and discharge process [3]. The largest volume change is observed for the anode material graphite, which is used in nearly all commercial cells. Graphite changes its volume by about 13% during complete lithiation [4]. Lithium Titanate Oxide (LTO), another anode material, undergoes a volume change of 0% during complete lithiation [5]. The different cathode materials also experience reversible volume changes by changing their volume between the fully lithiated and non-lithiated states. Lithium Nickel Cobalt Manganese (NMC) changes its volume by about 3%, Lithium Manganese Dioxide (LMO) about 7.5%, and Lithium Iron Phosphate (LFP)($LiFePO_4$) about 6.8% during a charge cycle [6]. Due to the different expansion rates of the used materials, a characteristic expansion curve can be found for each cell chemistry [7], [8], [9]. The reversible volume change results in additional stress on the cell components. Especially for the active materials in the cell, this stress can lead to damage in the form of microcracks. These microcracks in the active materials lead to a reduced electrical connection and thus to an increased internal resistance. In addition, the Solid Electrolyte Interphase (SEI) is damaged by mechanical stress. This damage leads to a steady increase of the SEI due to reformation and thus to an increase of the internal resistance [10], [11], [12]. So mechanical strains on the cell lead to accelerated aging and the consequent decline in cell performance. The following Table 1 shows a summary of the most common active materials used in lithium-ion batteries.

TABLE 1. The most important properties of common active materials.

Active material	Gravimetric energy density	Average voltage vs. Li^+	Volume change [%]
Anode materials			
Graphite	372 mAh g^{-1} [13]	0.1 V [13]	13% [4]
LTO	175 mAh g^{-1} [13]	1.55 V [13]	0% [5]
Cathode materials			
NMC	280 mAh g^{-1} [13]	3.7 V [13]	3% [6]
LMO	148 mAh g^{-1} [13]	4.1 V [13]	7.5% [6]
LFP	160 mAh g^{-1} [14]	3.4 V [13]	6.8% [6]

In addition, the volume change of the cell is influenced by further mechanisms. For example, the cell expands irreversibly during the SEI formation that takes place in the manufacturing process. During the formation process, this causes the overall cell to increase in thickness by approximately 3% [15]. In addition, the volume of the cell irreversibly increases over its lifetime due to aging mechanisms such as the growth of the SEI or lithium plating [16], [17]. Besides SEI growth, lithium plating is one of the major aging factors of lithium-ion cells. Lithium plating is the deposition of metallic lithium on the graphite anode. It mainly occurs by low temperatures, high charging current, and charging in the high State Of Charge (SOC) range [18], [19], [20]. This deposition is divided into a reversible part and an irreversible part. Lithium plating leads to a reduction of active lithium and mechanical stress on the anode and thus to an accelerated aging of the cell [21], [22]. In addition, lithium plating can lead to an internal short circuit of the battery by forming lithium dendrites [23], [24], [25]. Since lithium in the metallic form has a much higher volume than in the intercalated form, the deposition of metallic lithium leads to higher cell expansion [26]. Previous detection techniques use neutron diffraction [27], [28] or voltage relaxation techniques [29], [30], [31] to detect lithium plating.

The cathode material LFP is first mentioned in the literature in 1997 by Padhi et al. [32]. This cell chemistry uses a $LiFePO_4$ cathode. Compared to other cell chemistries, LFP has a lower achievable energy density of 160 mAh g^{-1} [14], however, it has significantly higher thermal stability and is much more environment-friendly due to the absence of metals such as cobalt. Due to their high operational safety and cheaper material value, LFP batteries are expected to find their use in safety-critical applications, such as the electrification of flying objects and automobiles or home storages. The A123 (AMP20M1HD-A) cells used in this work are composed of a $LiFePO_4$ cathode and a graphite anode. The following Fig. 1 shows the theoretical expansion behavior of these two materials depending on the degree of lithiation. Due to the chemical structure of graphite, a systematic intercalation of the lithium ions takes place. This intercalation can be divided into different stages depending on the degree of lithiation. Graphite staging leads to an expansion curve that is characteristic for grafit. This curve shows a high expansion at the beginning of lithiation (stage IV->III), an expansion plateau in the middle lithiation range (stage III(L) -> II), and a strong expansion again in the high lithiation range (stage II -> I). LFP, on the other hand, undergoes a linear volume increase during lithiation, i.e., during the phase change between $FePO_4$ to $LiFePO_4$ [6], [32], [33].

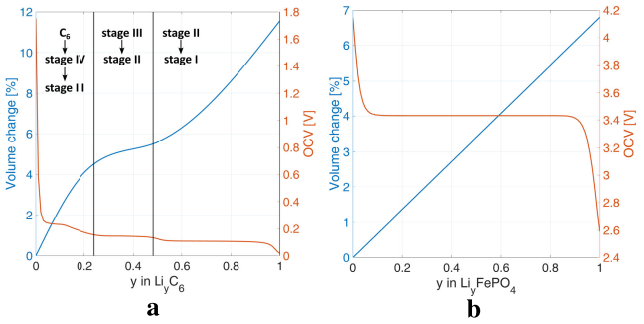

FIGURE 1. a) The expansion curve and the voltage curve of a graphite anode are shown; b) The expansion curve and the voltage curve of $LiFePO_4$ are show [33].

If graphite is used as anode material, two different phenomena are mainly caused by higher currents and lower temperatures. The first is that the entire anode is not lithiated homogeneously. More lithium is intercalated on the side facing the separator and a layer formation of different graphite stages within the anode occurs [34], [35], [36]. A second effect is the formation of overshooting graphite

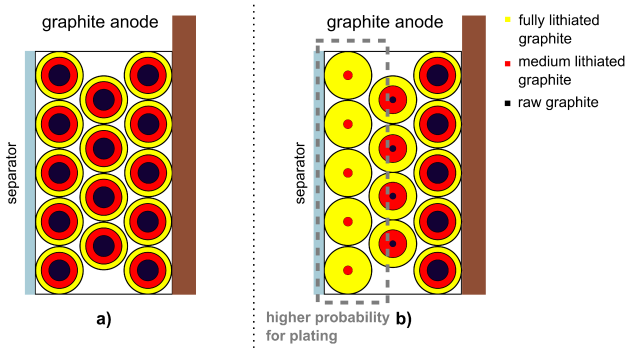

FIGURE 2. a) The formation of overshooting graphite stages inside the graphite grains is shown schematically b) The layer formation along the graphite anode is shown in a simplified way [38].

stages where the graphite solids become more lithiated in the surface region than in the core [37]. During relaxation, the lithium diffuses within the graphite bodies and also via galvanic corrosion [35] within the anode, causing a graphite state change and thus a change in volume until a state of equilibrium is reached. Since the expansion behavior of graphite is caused primarily by its state changes, both phenomena produce a relaxation of the cell expansion. This behavior can differ based on the SOC of the cell [38]. The following Fig. 2 illustrates the two phenomena described in a highly simplified form.

In the literature, there are several papers focusing on the expansion measurement of lithium-ion cells or the effects of this expansion. For example, structural changes in the cell can be recorded using XRD (X-ray diffraction) [39]. Furthermore, expansion of the cell usually results in increased pressure on its support or housing. This pressure can be measured to estimate the expansion of the cell [40], [41], [42]. There are also measurements that use a mechanical stylus to determine cell expansion [9]. Imaging microscope systems can also be used for specially prepared laboratory cells. With this system, the lithiation behavior and additionally the expansion behavior of the electrodes can be observed directly [43], [44]. In the work of Rieger et al. [45] a measurement setup is used, which measures the cell expansion at several locations of the cell. The setup operates with an accuracy of 2 µm. It is shown that the cell expansion can differ over the entire cell area and is especially high near the battery contacts. In addition, a relationship between temperature and cell expansion is shown. A lower temperature ensures a higher cell temperature. A post-mortem analysis of the cell also shows a correlation between the expansion and lithium plating. Jahn et al. [46] present in their work a method that matches the cell expansion to the voltage relaxation and thereby shows the expansion behavior of lithium plating. A mechanical probe with the resolution of 0.1 µm is used in this work. Also in this work, a relationship between expansion and lithium plating can be shown by comparing the expansion relaxation and voltage relaxation after charging the cell. Another work by Bauer et al. [38] investigates the quasi-equilibrium expansion of an NMC cell. For this purpose, the volume change of a cell is considered at a low current rate ($C/40$). The expansion of the cell is about 1.5% of the total thickness during a charge/discharge cycle. The measurement system used has an accuracy of 1 µm. In this work, it was also confirmed by half-cell measurements that a large part of the volume change is caused by the graphite anode. In addition, the expansion behavior during a Galvanostatic Intermittent Titration Technique (GITT) measurement is demonstrated. Here, the two phenomena of lithium plating and the formation of overshooting graphite stages can be related to cell expansion by looking at the relaxation behavior after the respective current pulses.

Laser interferometry is a common measurement method in dilatometry. It uses the superposition of light waves and the resulting interference signals to determine the change in length of a test path. Interferometric systems are usually based on the Michelson interferometer and achieve resolutions in the sub-nanometer range [47]. Other designs such as the Fabry-Pérot interferometer can also be found in the literature [48] and [49]. A distinction is made between homodyne interferometers, which use one light frequency for length determination [50], [51] and heterodyne interferometers, which use several light frequencies [52], [53]. Tolerances in the optical and electrical components and polarity mixing result in a non-linear measurement error [54]. A number of works in the literature are concerned with correction methods for non-linearities [55], [56], [57], [58]. In addition to non-linearities, inaccuracies also arise due to a change in environmental parameters such as temperature, humidity and air pressure, since these factors influence the wavelength of the laser light used. Work on this can be found in the literature, which corrects for the influence of the environmental parameters [59], [60].

Since the correlation between certain cell phenomena and cell expansion can be found in the literature, this paper presents a new measurement method that can determine cell expansion and the aging effects involved using short current pulses. The measurement method is first tested on a lithium iron phosphate cell. The expansion of a lithium iron phosphate cell experiences a decrease in the range from 30% SOC to 60% SOC. Here, only the iron phosphate cathode contributes to the cell expansion. Thus, the cell experiences a linear shrinkage. Since effects such as lithium plating lead to increased cell expansion, these can be directly detected by a measurement in this SOC range. Homodyne-Michelson interferometers as presented in work [61] and [62] offer a very high measurement accuracy of a few nanometers combined with a high measurement range. This makes an interferometric measurement setup well suited for building a laboratory system that is independent of cell shape and cell size. In addition, the high resolution of the interferometer makes it possible to detect even small expansions of the cell. This means that the expansion can be measured in response to a short current pulse, with a small amount of charge transferred. The combination of a short current pulse

and the high resolution of an interferometer setup sets this work apart from existing literature, as it allows the detection of aging effects such as lithium plating within a short measurement time. As a result, it should be possible to obtain a better insight into the phenomena shown by the literature such as lithium plating, SEI growth, or the formation of overshooting graphite stages. Early detection of conditions for ageing effects allows charging strategies to be adjusted before accelerated ageing of the cell occurs.

II. MATERIALS AND METHODS

A. POLARIZATION OPTICAL HOMODYNLASER INTERFEROMETER

The test system used in this work measures the expansion of a test specimen using an optical method from laser interferometry. Following the work of Hu. et al. [62] and Cui et al. [61], a common homodyne laser interferometer was constructed to allow measurement inside a climatic chamber (Memmert IP55). In addition, suitably high mechanical stability of the setup was ensured to minimize parasitic vibration effects. A software was developed, which preprocesses and evaluates the incoming signals accordingly. The interferometric method is explained below. The optical setup as well as the signal and data processing are described. Afterwards, the complete system is presented. The following Fig. 3 shows the schematic structure of the interferometer.

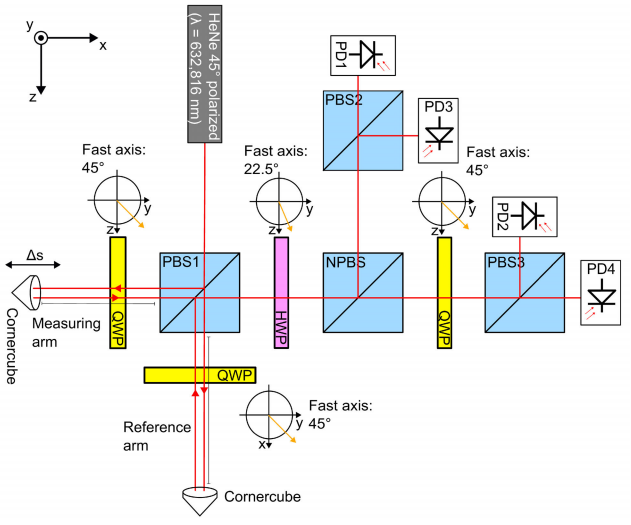

FIGURE 3. The figure shows schematically the optical structure of the interferometer system using a HeNe (helium-neon) laser of wavelength 632.816 nm**.**

A polarized HeNe laser with a wavelength of 632.816 nm and a power of 5 mW is used for the interferometer. This type of laser generates the light by energy state changes of the neon atoms and thus emits light of a fixed wavelength. They show high wavelength stability, which can be affected only by temperature variations within the laser. In addition, gas lasers generally have a very high coherence length even at high path length differences, which is essential for the formation of interference patterns [63], [64]. In the interferometer setup, this HeNe laser is used with a 45° polarization direction in the XY plane directed to the Polarizing Beam Splitter (PBS) cube PBS1. Due to the laser polarization, this cube splits the incoming laser light with equal intensity into a beam on the XZ plane (P-polarization) and a beam on the YX plane (S-polarization). This results in a reference arm whose distance to the PBS1 is kept constant and a measuring arm whose distance to the PBS1 is changed. This change in the measuring arm is the measured value of the interferometer. The divided light passes through a $\lambda/4$ plate (QWP) in both the measurement and reference arms, which causes the light that reflects back from the reflector to be rotated by 90° to the original polarity specified by the PBS1. As a result, the light from the PBS1 is now thrown out of the cube in a direction shifted by 90°, rather than in the direction of the light source. This simplifies the setup of the interferometer but is not necessary for the function. The laser beam exiting PBS1 is now a superposition of the light from the measurement and reference arms, on the P- and S-axes respectively. By the following $\lambda/2$ plate (HWP) with its fast axis at 22.5°, the light polarization is rotated by 45°. This 45° polarized light is now split by a Non Polarizing Beam Splitter (NBPS) and projected onto the two polarizing beam splitters PBS2 and PBS3. Here, one of the arms contains a $\lambda/4$ plate with its fast axis in the polarization direction of the incoming light, causing a phase shift of the incoming light beam by $\pi/4$. The light emerging from both PBS2 and PBS3 is measured by two Photodiodes (PD) each and converted into a voltage signal. In preprocessing, the photodiode voltages are amplified by an operational amplifier circuit with adjustable gain A_{1-4} and offset C_{1-4}. The adjustable gain and offset allows manual calibration of the signal amplitudes, and the signal offsets. By calibrating the measurement setup, the amplitudes of the signals and the offsets of the signals are adjusted so that approximately: $A_1 \approx A_2 \approx A_3 \approx A_4$; $C_1 \approx C_2 \approx C_3 \approx C_4$. In addition, a low-pass filter with the cut-off frequency of 1.6 Hz was used. This low-pass filter prevents disturbance from high-frequency mechanical vibration but limits the measurable velocity in the measurement path to 0.5 µm s^{-1}. This results in the following filtered four signals I_1, I_2, I_3, I_4:

$$I_1 = A_1 \cdot \sin(\Phi(t) + 0°) + C_1, \quad (1)$$

$$I_2 = A_2 \cdot \sin(\Phi(t) + 90°) + C_2, \quad (2)$$

$$I_3 = A_3 \cdot \sin(\Phi(t) + 180°) + C_3, \quad (3)$$

$$I_4 = A_4 \cdot \sin(\Phi(t) + 270°) + C_4. \quad (4)$$

The DC offset is mainly determined by the finesse of the interferometer and is similar in all four photodiodes. The phase shift of the signals equal to 90° in respectively results on one hand from the shift by 180° of the signals of a PBS with respect to each other and from the $\lambda/4$ platelets in front of PBS3. In the next step, the four signals are sampled using the NI-USB6003 DAQ Device at a sample rate of 100 *smp/s*. The signals I_1 and I_3, I_2 and I_4 are digitally subtracted from

each other respectively. The signals are heavily oversampled to allow digital filtering later. This results in the two digital quadrature signals $I_x(k)$ and $I_y(k)$ shifted by 90° and free of DC offset.

$$I_x(k) = I_1(k) - I_3(k) = (A_1 + A_3) \cdot \sin(\Phi(k)), \quad (5)$$
$$I_y(k) = I_2(k) - I_4(k) = (A_2 + A_4) \cdot \cos(\Phi(k)). \quad (6)$$

Since nonlinear errors can occur in an interferometer setup as a result of inaccuracies of the components and reflections from the surfaces, corrections are applied to the signals at this point. For this purpose, methods for error correction from work [62] and [65] are used. After error correction, using the two quadrature signals, the phase position Φ of the two signals concerning each other can be calculated as follows:

$$\Phi(k) = \arctan(\frac{I_x(k)}{I_y(k)}) \quad (7)$$

If the path length in the measuring arm is now changed by the value Δs, the following relationship results, considering the laser wavelength λ:

$$\Delta s(k) = \begin{cases} \frac{\Delta\Phi(k)}{4 \cdot \pi} \cdot \lambda = \frac{\Phi(k) - \Phi(k-1)}{4 \cdot \pi} \cdot \lambda. \\ \text{if } \Phi(k) - \Phi(k-1) < T \\ 0 \quad \text{if } \Phi(k) - \Phi(k-1) > T \end{cases} \quad (8)$$

where T is a fixed threshold value. This is selected in the region of $0.7 \cdot \pi$. The influence of the refractive index change was neglected. Since the presented measurement methodology aims at short measurement times, it can be assumed that the refractive index change has no significant influence on the measurement. The assembled interferometer was validated with the use of a piezoelectric stage. A resolution of approx. 10nm was determined.

B. EXPERIMENTAL SETUP

The presented interferometer is embedded in the measurement setup, with which it is possible to measure battery cells of different designs and cell chemistries. The great advantage of an interferometer setup in this form is the very high resolution in the nanometer range paired with a very high measuring range, which enables flexible measurement of different test specimens. The following Fig. 4 shows the measurement setup.

On the one hand, the presented interferometer system, designed as a compact measuring box, and on the other hand the mechanical probe of the company Keyence (GT2-PK12K, resolution 0.1 µm), are used. The mechanical probe has a resolution that is less accurate by a factor of ten and is therefore primarily used as a comparison system for function control but can also be used for long-term cyclization tests, where high accuracy is a minor requirement. In this work, the probe is not used. The whole system is mounted on a metal construction which is stably connected to the base plate. Attention was paid to fix the metal struts in a way that external vibrations are hardly transmitted. Since the

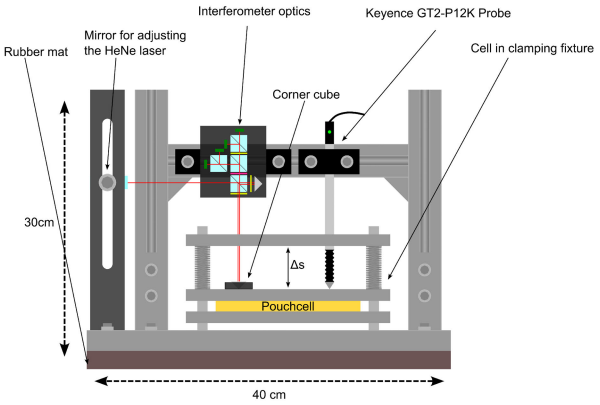

FIGURE 4. The entire measurement setup is shown. This measurement setup includes both the interferometer and a mechanical probe.

entire system is to be placed in a Memmert IP55 chamber, the HeNe laser was mounted parallel behind the metal construction as a light source for the interferometer. The laser is coupled in through a mirror construction, which enables easy adjustment of the beam. A slight vibration reduction to the climatic chamber floor is achieved with the use of a rubber mat. The surface to be measured is equipped with a retroreflector. A surface temperature sensor is used for temperature monitoring. Depending on the design of the cell holder, the measuring position may vary. In the case of the pouch cell measured, the two measuring points of the interferometer and probe are located in the front third in the direction of the cell contacts. The following figure 5 shows a picture of the measurement setup.

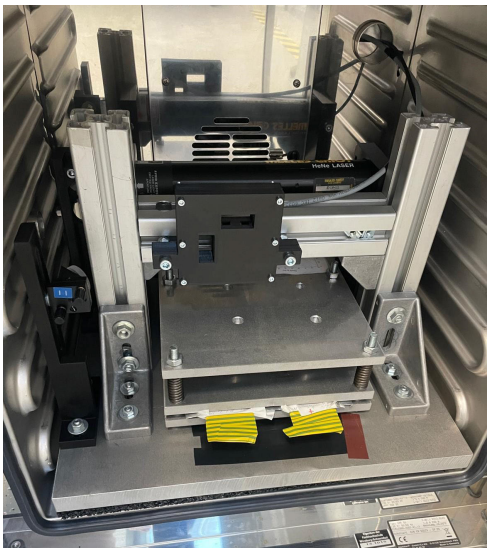

FIGURE 5. Photo of the measurement setup.

The AMP20M1HD-A pouch cell from A123 is measured in this work regarding its expansion. This cell consists of an LFP cathode paired with a graphite anode. A pouch cell was chosen to minimise the influence of the casing on the

measurement results. The cell has a nominal capacitance of 20 Ah and can be operated at 10C current at peak.

C. MEASUREMENT METHODOLOGY

In the next section, the new measurement methodology will be presented. Since the expansion measurement methodology is strongly based on the characteristic expansion curve of the LFP cell chemistry, an expansion curve was first recorded over a full charge and discharge cycle of the cell. The following Fig. 6 shows the expansion curve during a charge cycle and a discharge cycle plotted over the SOC. The curve was recorded from the interferometer setup presented. Additionally, the cell voltage is shown. During the measurement, the cell was charged and discharged at a constant current at an ambient temperature of 25 °C. The current rate is $\pm\frac{C}{20}(\widehat{=}1\,\mathrm{A})$. The cell was charged to the end-of-charge voltage of 3.6 V and discharged to the end-of-discharge voltage of 2.0 V specified in the data sheet. A pressure of 10psi was applied to the cell during all measurements. This value is specified as the pressure optimum in the data sheet.

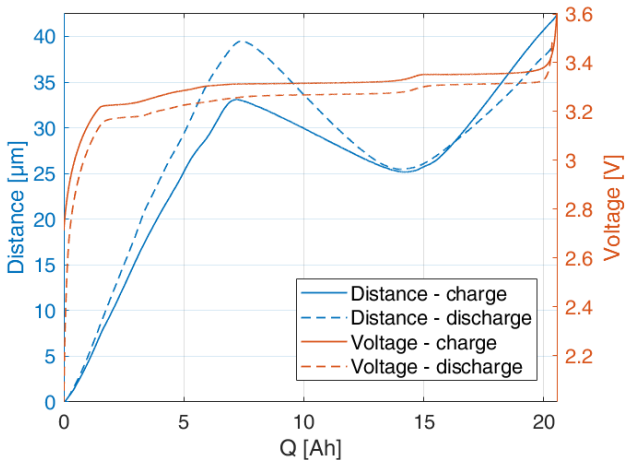

FIGURE 6. The expansion curve during a charge cycle and a discharge cycle of the AMP20M1HD-A cell is shown over the SOC. The cell voltage is also plotted. The cell was loaded with $C/20$.

It is observed that the cell experiences an overall expansion of about 42 µm and the expansion between charging and discharging is afflicted with hysteresis. It shows the typical expansion behavior of an LFP cell in having a decrease in cell thickness in the SOC range of 30% to 60%. In this region, the graphite is in its expansion plateau (cf. Fig. 1) and thus barely contributes to the total cell expansion. Here, the cell volume decreases as the thickness decrease of the $LiFePO_4$ cathode clearly outweighs. This result is also found in other works and can be confirmed by the literature [7]. The literature shows that effects such as the formation of overshooting graphite stages or lithium plating lead to increased cell expansion [38], [45], [46]. This relationship can be used to visualize the formation of overshooting graphite stages or lithium plating by the high resolution of the interferometer at a short time load current. This enables the detection of ageing mechanisms within short measuring times. Specifically, for this purpose, the expansion behavior is observed during a pulse measurement at 50% SOC with varying currents at different temperatures. It was ensured that the same amount of charge is transferred with each pulse to keep the theoretical volume change of the materials constant. An amount of charge of 1.33 Ah ($\widehat{=}6.7\%\ \Delta SOC$) was transferred during each current pulse. The cell was loaded with varying current intensity $I \in \{\pm 20\,\mathrm{A}, \pm 80\,\mathrm{A}\}$ with different time windows $t = \{240\,\mathrm{s}, 60\,\mathrm{s}\}$ at three different temperatures $T = \{10\,°\mathrm{C}, 20\,°\mathrm{C}, 30\,°\mathrm{C}\}$, both with positive and negative current. For each measurement the period of 1 min before the current pulse and 5 min after the current pulse is recorded.

III. RESULTS

First, shown graphically in Fig. 7 and presented numerically in Table 2, it can be seen that the cell undergoes shrinkage at a positive current pulse, as expected from the cyclization measurement. At a rather low current rate of 1C, shown in Fig. 7*a*), a linear shrinkage of the cell expansion can be seen. However, as the temperature decreases, the slope of this shrinkage also decreases, this is manifested primarily in a lower magnitude shrinkage of the cell at lower temperatures within the pulse duration. Immediately after the start of the charging current, a slight increase in cell expansion can be observed in the 10 °C measurement. The measurements at higher temperatures do not show this behavior. Looking at the relaxation after the 1C current pulse, it is noticeable that a slight relaxation of the expansion takes place at this low current rate. Lower cell temperature results in stronger expansion. If the current is now increased to 4C, shown in 7*b*), the cell responds to the start of the current pulse by expanding instead of shrinking. This behavior is stronger the lower the temperature is during the measurement. The cell expansion has an inflection point during the pulse duration and the cell begins to shrink. This shrinkage occurs earlier at higher temperatures, although almost no shrinkage can be measured at 10 °C ambient temperature. After the current is turned off, the cell exhibits strong relaxation behavior. This becomes stronger as the temperature decreases. The time constants of the relaxation to the 4C charge pulses were determined using an exponential fit. The determined time constants are summarized in Table 2. It is noticeable that the time constants

TABLE 2. Measurement results of the expansion measurement after a positive current pulse.

Ambient temperature:	10 °C	20 °C	30 °C
Overshoot at start of 1C:	15 nm	-	-
Overshoot at start of 4C:	890 nm	285 nm	77 nm
Expansion after relaxation 1C:	−1.33 µm	−1.70 µm	−1.85 µm
Expansion after relaxation 4C:	−1.02 µm	−1.51 µm	−1.82 µm
Time constant τ of relaxation 4C:	15.6 s	13.3 s	11.4 s
Difference after relaxation 1C (cf. 30°C):	520 nm	150 nm	-
Difference after relaxation 4C (cf. 30°C):	800 nm	310 nm	-
Max. Surface temperature difference:	0.43 °C	0.32 °C	0.25 °C
Temperature dependent expansion:	84 nm	63 nm	49 nm

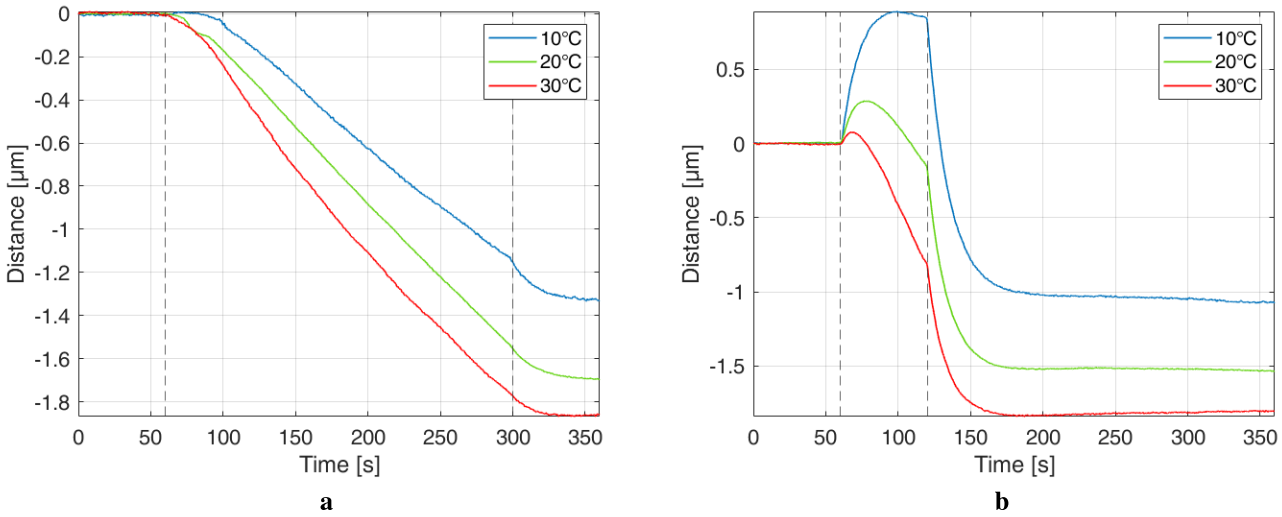

FIGURE 7. Expansion response to charge pulse measurement at different temperatures *a*) with a current of 1C, *b*) with a current of 4C.

are close to each other for all the temperature differences. Nevertheless, the time constants show a slight temperature dependence. At lower temperatures, the relaxation proceeds more slowly. In addition, a difference in cell expansion occurs after relaxation during the charging pulses, for both the 1C and 4C pulses. This phenomenon is amplified at high currents and low temperatures. It is also noticeable that there is a numerical correlation between the overshoot of the expansion signal at the start of the pulse and the difference after relaxation.

Looking at the response of the cell to the negative current pulses, shown graphically in Fig. 8 and presented numerically in Table 3, an increase in the cell's thickness can be seen, as expected from the cycling measurement. Similar to positive pulses, this expansion shows a nearly linear behavior at a 1C load, shown in Fig. 8*a*). However, the change in cell thickness increases slightly more than that for the positive current pulses. This is due to the hysteresis behavior, which can be seen in Fig. 6. Even with a negative current, the cell shows thickness relaxation, this becomes stronger the lower the temperature is. The measurement at 30 °C shows almost no relaxation. At higher current levels, shown in Fig. 8*b*), the total expansion of the cell increases to a higher value. However, this higher increase is also followed by a more significant relaxation of the cell thickness. Both the increase in cell expansion and the relaxation are stronger at low temperatures. The time constants of the relaxation after the 4C discharge pulses were determined same as for the positive pulses and summarized in Table 3. It can be seen that the time constants vary more than for the positive current pulses. The relaxation proceeds more slowly at low temperatures. Looking at the start of the discharge pulses, it is noticeable that the cell does not show any particular behavior at the start of the negative current pulse at both low and high currents.

In both measurements, an estimation for the error, of a temperature-dependent expansion of the cell, was performed. For this purpose, the cell was heated from 10 °C to 30 °C without an electrical connection, and the expansion was measured. Upon heating, the cell experiences a temperature-dependent expansion of 4 µm. This results in an expansion of 195 nm K^{-1} of the cell. The results are summarized in Table 2 and 3, respectively.

TABLE 3. Measurement results of the expansion measurement after a negative current pulse.

Ambient temperature:	10 °C	20 °C	30 °C
Max. Expansion -1C:	2.53 µm	2.57 µm	2.64 µm
Max. Expansion -4C:	5.26 µm	4.26 µm	3.66 µm
Expansion after relaxation 1C:	2.32 µm	2.50 µm	2.61 µm
Expansion after relaxation 4C:	2.96 µm	2.94 µm	2.90 µm
Time constant τ of relaxation 4C:	20.8 s	16.4 s	14.1 s
Difference after relaxation -1C (cf. 30°C):	290 nm	110 nm	-
Difference after relaxation -4C (cf. 30°C):	-	-	-
Max. Surface temperature difference:	0.35 °C	0.2 °C	0.15 °C
Temperature dependent expansion:	69 nm	39 nm	30 nm

IV. DISCUSSION

The presented measurement results in figure 7 and 8 prove that observation of anode effects is possible with method presented in this paper measuring the expansion response to a current pulse of a LFP cell at 50% SOC. Presumably, the two effects of lithium plating and the formation of overshooting graphite stages can be observed superposed. A clear separation and definite proof of the two effects is not yet possible with this measurement. By using established lithium plating detection methods, a correlation between expansion and lithium plating is intended to be established in future studies. The fact that the expansion overshoot only occurs during charging pulses, i.e. when the ions move in the direction of the graphite, and that the expansion overshoot shows a strong current and temperature dependence suggests that this effect has something to do with the deposition of

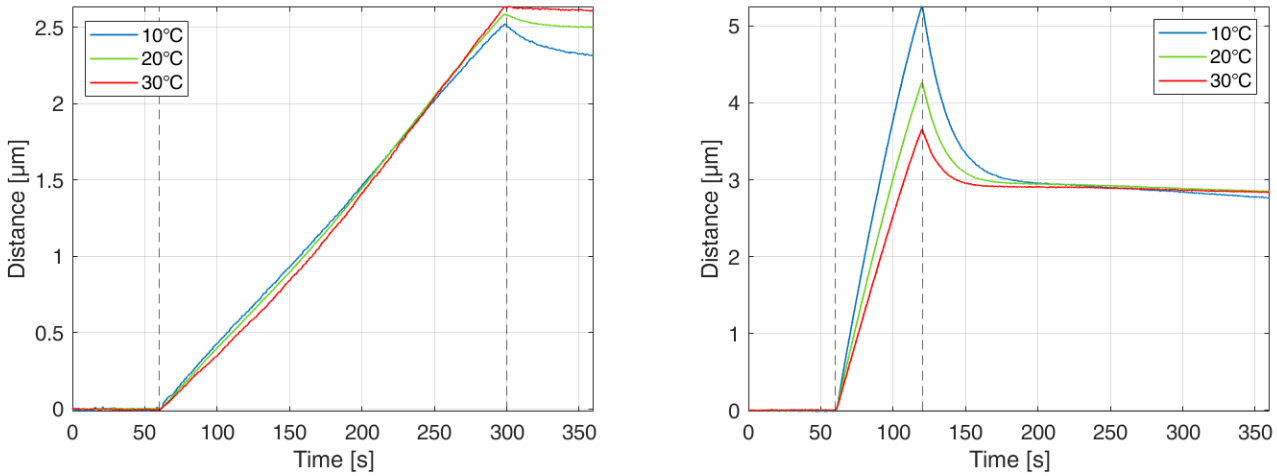

FIGURE 8. Expansion response to discharge pulse measurement at different temperatures *a*) with a current of −1C, *b*) with a current of −4C.

metallic lithium. Thus, it can be assumed that during a charge pulse with low temperatures and high currents, the diffusion rate of the graphite is not high enough to intercalate the incoming lithium into the solid. As a result, high graphite stages form at the edge of the particles, followed by a metallic lithium layer. If the load is switched off, the relaxation of the graphite stages is superimposed with the deposition of the metallic lithium layer. It can be assumed that the relaxation that takes place is related to the dissolution of the graphite stages. This is indicated by the fact that this relaxation also occurs during the discharge pulses so that the connection to lithium plating can be excluded. The expansion difference observed during the charging pulses, which occurs after relaxation, is probably related to the metallic lithium layer formed. It can be assumed that this expansion difference, as in work [46], will dissipate again within the next few hours, as the metallic lithium is intercalated in the anode.

V. CONCLUSION

In this work, the usability of an interferometer setup for cell expansion measurement was demonstrated. Through the interferometric measurement, the expansion phenomena of the battery cell can be recorded and evaluated with very high resolution. In addition, the very good spatial resolution of 10 nm allows the cell expansion to be detected even at low charge amounts transferred, which was not possible with existing test systems. Using a new measurement methodology that utilizes the expansion behavior of an LFP cell at 50% SOC, it was shown that effects such as the formation of overshooting graphite stages or lithium plating, can be recorded by evaluating the expansion response to temporally short current pulses. This behavior will be further explored in future measurements using known detection techniques. The works of [29] and [30] utilize voltage relaxation techniques to detect lithium plating. In future measurements, these methods can be used to establish a correlation between observed lithium plating and the expansion behavior highlighted in this study. As a technical application of this measurement methodology, if successfully developed and verified, a State Of Healt (SOH) determination could be performed using expansion measurement. In commercial applications where the measuring ranges are defined, it is conceivable to replace the expensive interferometer with a cheaper alternative such as capacitive sensors. This SOH estimation could be used in combination with known active-balancing systems such as in work [66]. This kind of system balances the cells using short current pulses. Here, the expansion response can be recorded and evaluated concerning the cell SOH. Furthermore, an investigation of other cell chemistries is interesting. These do not have the for LFP typical expansion curve, but it can be assumed that ageing effects such as lithium plating have a characteristic expansion behaviour and can also be detected in other cell chemistries. The investigation of other cell formats, especially pristamic cells, is also very interesting, as these are increasingly being used commercially. As possible improvements, a complete characterization of disturbing influences such as temperature fluctuations, vibrations and changes in the refractive index on the interferometer should be done. These disturbances manifest themselves in a slow drift of the expansion signal and therefore complicate a long-term measurement of the cell expansion. If long-term stability is achieved, the diffusion effects, which can still occur up to hours after the current pulse, can also be recorded and evaluated. This long-term observation of cell expansion can be used to better classify and evaluate the observed effects.

In this paper, a measurement methodology is presented that can record expansion effects occurring on the anode side, such as overshooting graphite stages or lithium plating in response to a short current pulse in a lithium iron phosphate cell. This is made possible by utilizing a highly-resolved interferometric measurement setup with a resolution of

approximately 10 nm. This work demonstrates the feasibility of assessing the expansion behavior of a lithium-ion cell within a short timeframe.

Author Contributions: Conceptualization, S.G. and G.B.; software, S.G. and T.H.; validation, A.Z., D.O. and S.B.; formal analysis, T.H.,A.Z., D.O. and S.B.; writing—original draft preparation, S.G.; writing—review and editing, T.H., D.O. and G.B; supervision, G.B. and A.Z.; funding acquisition, G.B. All authors have read and agreed to the published version of the manuscript.

Funding: This research was funded by the bavarian government (Hightech Agenda).

Conflicts of Interest: The authors declare no conflicts of interest.

REFERENCES

[1] J. Figgener, C. Hecht, D. Haberschusz, J. Bors, K. G. Spreuer, K.-P. Kairies, P. Stenzel, and D. U. Sauer, "The development of battery storage systems in Germany: A market review (status 2023)," 2023, *arXiv:2203.06762*.

[2] M. Li, J. Lu, Z. Chen, and K. Amine, "30 years of lithium-ion batteries," *Adv. Mater.*, vol. 30, no. 33, Aug. 2018, Art. no. 1800561.

[3] J. H. Lee, H. M. Lee, and S. Ahn, "Battery dimensional changes occurring during charge/discharge cycles—Thin rectangular lithium ion and polymer cells," *J. Power Sources*, vols. 119–121, pp. 833–837, Jun. 2003.

[4] S. Schweidler, L. de Biasi, A. Schiele, P. Hartmann, T. Brezesinski, and J. Janek, "Volume changes of graphite anodes revisited: A combined operando X-ray diffraction and in situ pressure analysis study," *J. Phys. Chem. C*, vol. 122, no. 16, pp. 8829–8835, Apr. 2018.

[5] T. Ohzuku, A. Ueda, and N. Yamamoto, "Zero-strain insertion material of $Li[Li_{1/3}Ti_{5/3}]O_4$ for rechargeable lithium cells," *J. Electrochem. Soc.*, vol. 142, no. 5, p. 1431, 1995.

[6] D. Ren, L. Xie, L. Wang, and X. He, "A practical approach to predict volume deformation of lithium-ion batteries from crystal structure changes of electrode materials," *Int. J. Energy Res.*, vol. 45, no. 5, pp. 7732–7740, Apr. 2021.

[7] E. Kwak, D. S. Son, S. Jeong, and K.-Y. Oh, "Characterization of the mechanical responses of a $LiFePO_4$ battery under different operating conditions," *J. Energy Storage*, vol. 28, Apr. 2020, Art. no. 101269.

[8] B. Rieger, S. Schlueter, S. V. Erhard, J. Schmalz, G. Reinhart, and A. Jossen, "Multi-scale investigation of thickness changes in a commercial pouch type lithium-ion battery," *J. Energy Storage*, vol. 6, pp. 213–221, May 2016.

[9] K.-Y. Oh, J. B. Siegel, L. Secondo, S. U. Kim, N. A. Samad, J. Qin, D. Anderson, K. Garikipati, A. Knobloch, B. I. Epureanu, C. W. Monroe, and A. Stefanopoulou, "Rate dependence of swelling in lithium-ion cells," *J. Power Sources*, vol. 267, pp. 197–202, Dec. 2014.

[10] D. Wang, X. Wu, Z. Wang, and L. Chen, "Cracking causing cyclic instability of $LiFePO_4$ cathode material," *J. Power Sources*, vol. 140, no. 1, pp. 125–128, Jan. 2005.

[11] A. Mukhopadhyay and B. W. Sheldon, "Deformation and stress in electrode materials for Li-ion batteries," *Prog. Mater. Sci.*, vol. 63, pp. 58–116, Jun. 2014.

[12] A. O. Kondrakov, A. Schmidt, J. Xu, H. Geßwein, R. Mönig, P. Hartmann, H. Sommer, T. Brezesinski, and J. Janek, "Anisotropic lattice strain and mechanical degradation of high- and low-nickel NCM cathode materials for Li-ion batteries," *J. Phys. Chem. C*, vol. 121, no. 6, pp. 3286–3294, Feb. 2017.

[13] N. Nitta, F. Wu, J. T. Lee, and G. Yushin, "Li-ion battery materials: Present and future," *Mater. Today*, vol. 18, no. 5, pp. 252–264, Jun. 2015.

[14] R. Korthauer, *Lithium-Ion Batteries: Basics and Applications*. Berlin, Germany: Springer, Aug. 2018.

[15] M. Hahn, H. Buqa, P. W. Ruch, D. Goers, M. E. Spahr, J. Ufheil, P. Novák, and R. Kötz, "A dilatometric study of lithium intercalation into powder-type graphite electrodes," *Electrochem. Solid-State Lett.*, vol. 11, no. 9, p. A151, 2008.

[16] J. Cannarella and C. B. Arnold, "State of health and charge measurements in lithium-ion batteries using mechanical stress," *J. Power Sources*, vol. 269, pp. 7–14, Dec. 2014.

[17] M. Lu, H. Cheng, and Y. Yang, "A comparison of solid electrolyte interphase (SEI) on the artificial graphite anode of the aged and cycled commercial lithium ion cells," *Electrochimica Acta*, vol. 53, no. 9, pp. 3539–3546, Mar. 2008.

[18] Q. Liu, C. Du, B. Shen, P. Zuo, X. Cheng, Y. Ma, G. Yin, and Y. Gao, "Understanding undesirable anode lithium plating issues in lithium-ion batteries," *RSC Adv.*, vol. 6, no. 91, pp. 88683–88700, 2016.

[19] C. V. Lüders, *Experimentelle und Simulative Untersuchung von Lithium-Plating und Lithium-Stripping in Lithium-Ionen-Zellen*. Munich: Technische Universität München, 2019.

[20] B.-I. Hogg, T. Waldmann, and M. Wohlfahrt-Mehrens, "4-electrode full cells for operando Li^+ activity measurements and prevention of Li deposition in Li-ion cells," *J. Electrochem. Soc.*, vol. 167, no. 9, Jan. 2020, Art. no. 090525.

[21] M. Petzl, M. Kasper, and M. A. Danzer, "Lithium plating in a commercial lithium-ion battery—A low-temperature aging study," *J. Power Sources*, vol. 275, pp. 799–807, Feb. 2015.

[22] U. R. Koleti, A. Rajan, C. Tan, S. Moharana, T. Q. Dinh, and J. Marco, "A study on the influence of lithium plating on battery degradation," *Energies*, vol. 13, no. 13, p. 3458, Jul. 2020.

[23] C. Hogrefe, T. Waldmann, M. Hölzle, and M. Wohlfahrt-Mehrens, "Direct observation of internal short circuits by lithium dendrites in cross-sectional lithium-ion in situ full cells," *J. Power Sources*, vol. 556, Feb. 2023, Art. no. 232391.

[24] M. Rosso, C. Brissot, A. Teyssot, M. Dollé, L. Sannier, J.-M. Tarascon, R. Bouchet, and S. Lascaud, "Dendrite short-circuit and fuse effect on Li/polymer/Li cells," *Electrochimica Acta*, vol. 51, no. 25, pp. 5334–5340, Jul. 2006.

[25] L. Huang, L. Liu, L. Lu, X. Feng, X. Han, W. Li, M. Zhang, D. Li, X. Liu, D. U. Sauer, and M. Ouyang, "A review of the internal short circuit mechanism in lithium-ion batteries: Inducement, detection and prevention," *Int. J. Energy Res.*, vol. 45, no. 11, pp. 15797–15831, Sep. 2021.

[26] B. Bitzer and A. Gruhle, "A new method for detecting lithium plating by measuring the cell thickness," *J. Power Sources*, vol. 262, pp. 297–302, Sep. 2014.

[27] V. Zinth, C. von Lüders, M. Hofmann, J. Hattendorff, I. Buchberger, S. Erhard, J. Rebelo-Kornmeier, A. Jossen, and R. Gilles, "Lithium plating in lithium-ion batteries at sub-ambient temperatures investigated by in situ neutron diffraction," *J. Power Sources*, vol. 271, pp. 152–159, Dec. 2014.

[28] V. Zinth, C. von Lüders, J. Wilhelm, S. V. Erhard, M. Hofmann, S. Seidlmayer, J. Rebelo-Kornmeier, W. Gan, A. Jossen, and R. Gilles, "Inhomogeneity and relaxation phenomena in the graphite anode of a lithium-ion battery probed by in situ neutron diffraction," *J. Power Sources*, vol. 361, pp. 54–60, Sep. 2017.

[29] M. Petzl and M. A. Danzer, "Nondestructive detection, characterization, and quantification of lithium plating in commercial lithium-ion batteries," *J. Power Sources*, vol. 254, pp. 80–87, May 2014.

[30] I. D. Campbell, M. Marzook, M. Marinescu, and G. J. Offer, "How observable is lithium plating? Differential voltage analysis to identify and quantify lithium plating following fast charging of cold lithium-ion batteries," *J. Electrochem. Soc.*, vol. 166, no. 4, pp. A725–A739, 2019.

[31] T. Hein, D. Oeser, A. Ziegler, D. Montesinos-Miracle, and A. Ackva, "Aging determination of series-connected lithium-ion cells independent of module design," *Batteries*, vol. 9, no. 3, p. 172, Mar. 2023.

[32] A. K. Padhi, K. Nanjundaswamy, and J. B. Goodenough, "Phospho-olivines as positive-electrode materials for rechargeable lithium batteries," *J. Electrochem. Soc.*, vol. 144, no. 4, p. 1188, 1997.

[33] D. Clerici, F. Mocera, and A. Somà, "Experimental characterization of lithium-ion cell strain using laser sensors," *Energies*, vol. 14, no. 19, p. 6281, Oct. 2021.

[34] D. P. Finegan, A. Quinn, D. S. Wragg, A. M. Colclasure, X. Lu, C. Tan, T. M. M. Heenan, R. Jervis, D. J. L. Brett, S. Das, T. Gao, D. A. Cogswell, M. Z. Bazant, M. Di Michiel, S. Checchia, P. R. Shearing, and K. Smith, "Spatial dynamics of lithiation and lithium plating during high-rate operation of graphite electrodes," *Energy Environ. Sci.*, vol. 13, no. 8, pp. 2570–2584, 2020.

[35] Y. Chen, K.-H. Chen, A. J. Sanchez, E. Kazyak, V. Goel, Y. Gorlin, J. Christensen, K. Thornton, and N. P. Dasgupta, "Operando video microscopy of Li plating and re-intercalation on graphite anodes during fast charging," *J. Mater. Chem. A*, vol. 9, no. 41, pp. 23522–23536, 2021.

[36] S. J. Harris, A. Timmons, D. R. Baker, and C. Monroe, "Direct in situ measurements of Li transport in Li-ion battery negative electrodes," *Chem. Phys. Lett.*, vol. 485, nos. 4–6, pp. 265–274, Jan. 2010.

[37] M. Heß and P. Novák, "Shrinking annuli mechanism and stage-dependent rate capability of thin-layer graphite electrodes for lithium-ion batteries," *Electrochimica Acta*, vol. 106, pp. 149–158, Sep. 2013.

[38] M. Bauer, M. Wachtler, H. Stöwe, J. V. Persson, and M. A. Danzer, "Understanding the dilation and dilation relaxation behavior of graphite-based lithium-ion cells," *J. Power Sources*, vol. 317, pp. 93–102, Jun. 2016.

[39] N. A. Cañas, P. Einsiedel, O. T. Freitag, C. Heim, M. Steinhauer, D.-W. Park, and K. A. Friedrich, "Operando X-ray diffraction during battery cycling at elevated temperatures: A quantitative analysis of lithium-graphite intercalation compounds," *Carbon*, vol. 116, pp. 255–263, May 2017.

[40] R. Hickey and T. M. Jahns, "Measuring individual battery dimensional changes for state-of-charge estimation using strain gauge sensors," in *Proc. IEEE Energy Convers. Congr. Expo. (ECCE)*, Sep. 2019, pp. 2460–2465.

[41] L. K. Willenberg, P. Dechent, G. Fuchs, D. U. Sauer, and E. Figgemeier, "High-precision monitoring of volume change of commercial lithium-ion batteries by using strain gauges," *Sustainability*, vol. 12, no. 2, p. 557, Jan. 2020.

[42] C. Bae, A. Manandhar, P. Kiesel, and A. Raghavan, "Monitoring the strain evolution of lithium-ion battery electrodes using an optical fiber Bragg grating sensor," *Energy Technol.*, vol. 4, no. 7, pp. 851–855, Jul. 2016.

[43] K. E. Thomas-Alyea, C. Jung, R. B. Smith, and M. Z. Bazant, "In situ observation and mathematical modeling of lithium distribution within graphite," *J. Electrochem. Soc.*, vol. 164, no. 11, pp. E3063–E3072, 2017.

[44] C. Hogrefe, T. Waldmann, M. B. Molinero, L. Wildner, P. Axmann, and M. Wohlfahrt-Mehrens, "Cross-sectional in situ optical microscopy with simultaneous electrochemical measurements for lithium-ion full cells," *J. Electrochem. Soc.*, vol. 169, no. 5, May 2022, Art. no. 050519.

[45] B. Rieger, S. F. Schuster, S. V. Erhard, P. J. Osswald, A. Rheinfeld, C. Willmann, and A. Jossen, "Multi-directional laser scanning as innovative method to detect local cell damage during fast charging of lithium-ion cells," *J. Energy Storage*, vol. 8, pp. 1–5, Nov. 2016.

[46] L. Jahn, F. Katzer, and M. A. Danzer, "Combined dilatometry and voltage analysis for a reliable detection of lithium deposition on graphitic anodes," *J. Power Sources*, vol. 520, Feb. 2022, Art. no. 230870.

[47] E. G. Wolff and R. C. Savedra, "Precision interferometric dilatometer," *Rev. Sci. Instrum.*, vol. 56, no. 7, pp. 1313–1319, Jul. 1985.

[48] T. Yoshino, K. Kurosawa, K. Itoh, and T. Ose, "Fiber-optic Fabry–Pérot interferometer and its sensor applications," *IEEE J. Quantum Electron.*, vol. QE-18, no. 10, pp. 1624–1633, Oct. 1982.

[49] M. Islam, M. Ali, M.-H. Lai, K.-S. Lim, and H. Ahmad, "Chronology of Fabry–Pérot interferometer fiber-optic sensors and their applications: A review," *Sensors*, vol. 14, no. 4, pp. 7451–7488, Apr. 2014.

[50] T. Požar, P. Gregorčič, and J. Možina, "A precise and wide-dynamic-range displacement-measuring homodyne quadrature laser interferometer," *Appl. Phys. B, Lasers Opt.*, vol. 105, no. 3, pp. 575–582, Nov. 2011.

[51] S. Rerucha, Z. Buchta, M. Sarbort, J. Lazar, and O. Cip, "Detection of interference phase by digital computation of quadrature signals in homodyne laser interferometry," *Sensors*, vol. 12, no. 10, pp. 14095–14112, Oct. 2012.

[52] K.-N. Joo, J. D. Ellis, J. W. Spronck, P. J. M. van Kan, and R. H. M. Schmidt, "Simple heterodyne laser interferometer with subnanometer periodic errors," *Opt. Lett.*, vol. 34, no. 3, pp. 288–386, Feb. 2009.

[53] G. Straube, J. S. F. Calderón, I. Ortlepp, R. Füßl, and E. Manske, "A heterodyne interferometer with separated beam paths for high-precision displacement and angular measurements," *Nanomanufacturing Metrol.*, vol. 4, no. 3, pp. 200–207, Sep. 2021.

[54] C.-M. Wu, C.-S. Su, and G.-S. Peng, "Correction of nonlinearity in one-frequency optical interferometry," *Meas. Sci. Technol.*, vol. 7, no. 4, pp. 520–524, Apr. 1996.

[55] P. L. M. Heydemann, "Determination and correction of quadrature fringe measurement errors in interferometers," *Appl. Opt.*, vol. 20, no. 19, p. 3382, Oct. 1981.

[56] T. Eom, J. Kim, and K. Jeong, "The dynamic compensation of nonlinearity in a homodyne laser interferometer," *Meas. Sci. Technol.*, vol. 12, no. 10, pp. 1734–1738, Sep. 2001.

[57] P.-C. Hu, F. Pollinger, K. Meiners-Hagen, H.-X. Yang, and A. Abou-Zeid, "Fine correction of nonlinearity in homodyne interferometry," *Proc. SPIE*, vol. 7544, Dec. 2010, Art. no. 75444E.

[58] J. Ahn, J.-A. Kim, C.-S. Kang, J. W. Kim, and S. Kim, "A passive method to compensate nonlinearity in a homodyne interferometer," *Opt. Exp.*, vol. 17, no. 25, p. 23299, Dec. 2009.

[59] J. Lazar, O. Číp, M. Čížek, J. Hrabina, and Z. Buchta, "Suppression of air refractive index variations in high-resolution interferometry," *Sensors*, vol. 11, no. 8, pp. 7644–7655, Aug. 2011.

[60] Y.-S. Jang and S.-W. Kim, "Compensation of the refractive index of air in laser interferometer for distance measurement: A review," *Int. J. Precis. Eng. Manuf.*, vol. 18, no. 12, pp. 1881–1890, Dec. 2017.

[61] J. Cui, Z. He, J. Tan, and T. Sun, "Realization of a robust homodyne quadrature laser interferometer by performing wave plate yawing to realize ultra-low error sensitivity," *Opt. Exp.*, vol. 24, no. 20, p. 23505, 2016.

[62] P. Hu, J. Zhu, X. Guo, and J. Tan, "Compensation for the variable cyclic error in homodyne laser interferometers," *Sensors*, vol. 15, no. 2, pp. 3090–3106, Jan. 2015.

[63] K. R. Espinoza, "Helium neon lasers: Literature research paper helium neon lasers," Willamette Univ., Salem, Oregon, Tech. Rep., 2017, doi: 10.13140/RG.2.2.12816.87049.

[64] L. Allen and D. Jones, "The helium-neon laser," *Adv. Phys.*, vol. 14, no. 56, pp. 479–519, 1965.

[65] C. H. Wang, A. T. Augousti, and J. Mason, "Real time evaluation and correction of nonlinear errors in single frequency interferometers," *Trans. Inst. Meas. Control*, vol. 22, no. 5, pp. 405–412, May 2000.

[66] A. Ziegler, "Possibilities and limitations of active battery management systems for lithium-ion batteries," M.S. thesis, Departament d'Enginyeria Elèctrica, UPC, Barcelona, 2022.

SEBASTIAN GIELINGER was born in Ochsenfurt, Germany, in 1997. He received the master's degree in electrical engineering from the Technical University of Applied Sciences Würzburg-Schweinfurt (THWS), in 2022. Since April 2022, he has been a Research Assistant with the Technology Transfer Center for Electromobility (TTZ-EMO), Bad Neustadt an der Saale. As part of THWS, this research institute forms the link between the university and industry in the areas of E-mobility, energy storage, and energy transition. Since 2022, he has been in the field of battery technology and focusing on the topic "Expansion measurement of lithium-based energy storages." Researching battery expansion shall provide a better understanding of the aging mechanisms of lithium-ion cells. Within this topic, he develops software, hardware, and algorithms in the field of optical metrology.

THIEMO HEIN was born in Schweinfurt, Germany, in 1995. He received the M.Eng. degree in electrical engineering from the Technical University of Applied Sciences Würzburg-Schweinfurt (THWS), in 2019. He is currently a Research Assistant with the Technology Transfer Center for Electromobility (TTZ-EMO), Bad Neustadt an der Saale. This research institute is part of THWS, with a focus on many areas of E-mobility, energy system transformation, and energy efficiency. In 2021, he started writing the Ph.D. thesis in cooperation with the Polytechnic University of Catalonia (UPC), Barcelona, Spain, in the field of intelligent balancing algorithms. His research interests include control strategies and power electronics for battery systems and the investigation of battery aging.

ANDREAS ZIEGLER was born in Werneck, Germany, in 1993. He received the M.Eng. degree in electrical engineering from the Technical University of Applied Sciences Würzburg-Schweinfurt (THWS), in 2017. He is currently a Research Assistant and the Head of the Department of the Technology Transfer Center for Electromobility (TTZ-EMO), Department of "Battery Systems," Bad Neustadt an der Saale. This research institute is part of THWS, with a focus on many areas of E-mobility, energy system transformation, and energy efficiency. In 2019, he started writing the Ph.D. thesis in cooperation with the Polytechnic University of Catalonia (UPC), Barcelona, Spain, in the field of intelligent battery management, which he successfully completed, in 2022. He develops hardware, software, and algorithms for active cell balancing and evaluates the advantages and disadvantages of complex battery management systems.

DAVID OESER was born in Schweinfurt, Germany, in 1992. He received the M.Eng. degree in electrical engineering from the Technical University of Applied Sciences Würzburg-Schweinfurt (THWS), in 2017. He is currently a Research Assistant with the Technology Transfer Center for Electromobility (TTZ-EMO), Department "Battery Systems," Bad Neustadt an der Saale. This research institute is part of THWS, with a focus on many areas of E-mobility, energy system transformation, and energy efficiency. In 2019, he started writing the Ph.D. thesis in cooperation with the Polytechnic University of Catalonia (UPC), Barcelona, Spain, in the field of battery aging, which he successfully completed, in 2022. His work includes aging tests of single cells and battery modules and their evaluation.

SEBASTIAN BREITFELDER was born in Würzburg, Germany, in 2000. He received the bachelor's degree in functional materials from the University of Würzburg, in 2022. He is currently pursuing the master's degree in electrical engineering. He is also an Auxiliary Scientist with the Technology Transfer Center for Electromobility (TTZ-EMO), Bad Neustadt an der Saale. His research interest includes investigating the possibilities of lithium-plating detection.

GUNTHER BOHN received the Diploma degree in electrical engineering with the Friedrich-Alexander University of Erlangen-Nürnberg, in 1995, and the Ph.D. degree from the Institute of Optics, in 1998. He has been a Professor and the Head of the Optoelectronics Laboratory, Faculty of Electrical Engineering, Technical University of Applied Sciences Würzburg-Schweinfurt (THWS), since 2004. From 1999 to 2004, he was the Team Leader and the Project Manager of Robert BOSCH GmbH. He is also a Contributing Professor with the Technology Transfer Center for Electromobility (TTZ-EMO), where he develops methods for high-precision optical measurement of the expansion of lithium-ion batteries during charging and discharging. His research interests include accumulators and optical inspection systems.